Synthesis, Crystal Structure, Crystal Chemistry, and Magnetic Properties of $PbMBO_4$ (M = Cr, Mn, Fe): A New Structure Type Exhibiting One- Dimensional Magnetism

H. Park, R. Lam, J. E. Greedan,* and J. Barbier*

Department of Chemistry and Brockhouse Institute for Materials Research, McMaster University, Hamilton, Ontario, L8S 4M1 Canada

Received December 5, 2002. Revised Manuscript Received February 21, 2003

The crystal chemistry of a new structure type found in the Pb−M−B−O system, $PbMBO_4$ (M = Al, Ga), was extended to include M = Cr, Mn, and Fe. Extension to other trivalent ions, such as Ti, V, Co, Sc, In, and Y, failed for various reasons. Single crystals were grown from a PbO flux for M = Mn and Fe and the crystal structures were solved from X-ray single-crystal diffraction data. For M = Cr, the structure was refined from neutron powder diffraction data. The crystal structure is described in *Pnma* and features chains of edge-sharing MO_6 octahedra extended along the *b*-axis. Rigid, planar BO_3 groups bridge the MO_6 octahedra both within and between the chains, forcing the two M−O−M bridging angles involved in the shared edge to be highly asymmetric and constraining the M−M distances to be roughly constant at 2.97 Å. In all cases, one-dimensional short-range magnetic correlations were observed in the magnetic susceptibility data which were antiferromagnetic for M = Cr and Fe and ferromagnetic for M = Mn. Values for the intrachain exchange, J/k_B, were extracted from fits to standard models and were −4, −26, and +11 K for M = Cr, Fe, and Mn, respectively. Long-range order was observed below 8.3, 31, and 125 K for M = Cr, Mn, and Fe, respectively, and magnetic structures were refined from neutron powder diffraction data. $PbCrBO_4$ and $PbFeBO_4$ both show antiferromagnetic long-range order with the **b**-axis antiferromagnetic chains coupled ferromagnetically, while for $PbMnBO_4$ both intra- and interchain couplings are ferromagnetic. Thus, this latter material is a rare example of a ferromagnetic insulator. Attempts to rationalize the observed intrachain J/k_B values by reference to magneto-structural correlations were largely unsuccessful due to a lack of appropriate model compounds.

Introduction

The crystal chemistry of metal borates, both as natural minerals and as synthetic materials with potentially useful optical properties, is of continuing interest.[1] A huge variety of structures are known due in part to the dual bonding modes for the borate group, that is, either as BO_4^{5-} tetrahedra or BO_3^{3-} triangles, and also to the condensation of these units into chains, layers, and frameworks.[2] Recently, a new structure type of composition $PbMBO_4$ has been discovered in the Pb−Ga(Al)−B−O systems, namely, $PbGa(Al)BO_4$.[3,4] In these materials, linear chains of edge-sharing Ga(Al)−O octahedra are linked by BO_3^{3-} and PbO_4^{6-} groups. The interchain M−M separation is ∼5.45 Å while the intrachain M−M distance is ∼2.97 Å. Well-isolated chains of this type are fairly rare in oxide chemistry, one well-known example being the spin-Peierls compound, $CuGeO_3$.[5] It would be of particular interest if transition metal ions could be substituted for $Ga(Al)^{3+}$ in the $PbMBO_4$ structure, as one-dimensional magnetic correlations would then be anticipated. In this work, efforts are described to explore the crystal chemistry of this new structure type for trivalent 3d transition elements, especially M = Ti, V, Cr, Mn, Fe, and Co, and the larger trivalent elements such as Sc, Y, and In. The magnetic properties are reported, including the determination of the magnetic structure of the stable phases.

Experimental Section

Solid-State Syntheses. *M = Cr, Mn, and Fe.* Attempts to prepare the $PbMBO_4$ compounds (M = Cr, Mn, Fe) by reacting stoichiometric mixtures of PbO, M_2O_3, and $B(OH)_3$ powders failed due to the initial formation of low-melting lead borates (e.g., $Pb_2B_2O_5$ with a melting point of 495 °C). An alternate synthesis was therefore chosen based on the solid-state reactions between PbO and the pre-reacted MBO_3 compounds.

The $CrBO_3$ and $FeBO_3$ compounds were readily synthesized from stoichiometric mixtures of Cr_2O_3 (prepared by decomposition of $Cr(NO_3)_3{\cdot}9H_2O$ (98.9%, J.T. Baker) on a hot plate), Fe_2O_3 (reagent grade, Fisher), and $B(OH)_3$ (99.99%, Alfa Aesar). The mixtures were heated to 800 °C in air for 1−2 days and the purity of the products was checked by powder X-ray diffraction (Guinier-Hägg camera, Cu $K\alpha_1$ radiation, Si internal standard). In the case of M = Mn, the reaction of Mn_2O_3 (obtained by heating MnO_2 (99.9%, J.T. Baker) at 800 °C in

* Corresponding authors.

(1) Becker, P. *Adv. Mater.* **1998**, *10*, 979.
(2) Becker, P. *Z. Kristallogr.* **2001**, *216*, 523.
(3) Park, H.; Barbier, J. *Acta Crystallogr.* **2001**, *E57*, 82.
(4) Park, H.; Barbier, J.; Hammond, R. P. *Solid State Sci.*, **2003**, in press.
(5) Otto, H. H.; Wolfram, H. Z. *Kristallogr.* **2002**, *217*, 431.

10.1021/cm0217452 CCC: $25.00
Published on Web 03/28/2003

air for 1 day) with $B(OH)_3$ did not produce $MnBO_3$ but a mixture of $Mn_2BO_4 + {}^1/_2B_2O_3$, which was used as such. The impossibility to synthesize $MnBO_3$ contradicts a previous report[6] but agrees with a more recent study of the Mn_2BO_4 compound.[7]

The $PbO + MBO_3 \rightarrow PbMBO_4$ reactions were carried out in air for M = Mn, Fe and under high-purity argon for M = Cr to prevent the oxidation of Cr(III) to Cr(VI) and the formation of $PbCrO_4$. Small pellets (0.5 g) of the stoichiometric $PbO + MBO_3$ mixtures were heated to 800−850 °C for several days with intermediate re-mixings, and the progress of the reactions was followed by powder X-ray diffraction. All reactions were carried out in furnaces contained within fume hoods to minimize exposure to PbO vapors. No significant evaporation of PbO occurred at the temperatures used for the solid-state reactions. The $PbMBO_4$ compounds were obtained as dark green (M = Cr, Fe) and red-brown (M = Mn) microcrystalline powders. Their X-ray powder patterns were fully indexed on the same orthorhombic unit cell as that previously determined for $PbGaBO_4$.[3]

The larger $PbCrBO_4$ sample (5 g) used for the powder neutron diffraction experiments was synthesized as just described with the only difference that boric acid enriched in ^{11}B (99.27% from Eagle Picher) was used to minimize the absorption of neutrons by the ^{10}B nuclei.

M = Ti, V, and Co. Attempts were made to prepare the $PbMBO_4$ phase with other transition metals for which the +3 state is also stable in oxides, namely, Ti, V, and Co. In all three cases these efforts were unsuccessful. For M = Ti and V, PbO was reacted with $TiBO_3$ and VBO_3 under vacuum in sealed quartz ampules and, in both cases, the reaction products indicated that oxidation/reduction had occurred. In the case of M = Ti, elemental Pb was found among the products together with $PbTiO_3$ perovskite and, for M = V, the major crystalline product was $Pb_3V_2O_8$ where V is of course in the +5 state. The attempt to synthesize the M = Co compound involved a Co(+2) borate in the starting mixture along with PbO and 1 atm of O_2 gas. The principal crystalline product was Co_3O_4, which indicates that these conditions are insufficient to fully oxidize Co to the desired +3 state. It is possible that use of higher oxygen pressures could be successful using this reaction scheme.

M = Sc, Y, and In. Finally, the larger trivalent ions Sc^{3+}, Y^{3+}, and In^{3+} also form many stable oxides in which they occur in octahedral coordination. Unfortunately, reactions between $ScBO_3$, YBO_3, $InBO_3$, and PbO did not result in the formation of the $PbMBO_4$ phases. For instance, heating a stoichiometric mixture of PbO and $ScBO_3$ powders at 725 °C overnight yielded Sc_2O_3 as the only crystalline phase mixed with a Pb borate glass.

Single-Crystal Growth. Small single crystals of $PbMnBO_4$ and $PbFeBO_4$ were successfully grown in air using excess PbO as a flux. Mixtures with molar compositions of $4PbO-M_2O_3-2B(OH)_3$ ($PbMnBO_4$: 9.123 g of PbO + 1.613 g of Mn_2O_3 + 1.264 g of $B(OH)_3$; $PbFeBO_4$: 9.109 g of PbO + 1.629 g of Fe_2O_3 + 1.262 g of $B(OH)_3$) were melted at 1000 °C in a covered platinum crucible, held at that temperature for 2−3 h, slowly cooled to 500 °C at a rate of 3 °C/h, and finally quenched in air. After dissolution of the excess PbO in 1 M HNO_3(aq) at room temperature, large yields of clear, sub-millimeter size, prismatic crystals were recovered for both $PbMnBO_4$ (dark red) and $PbFeBO_4$ (dark green). In the case of the Mn compound, a small amount of black needles of $Pb_3Mn_7O_{15}$[8,9] was also recovered due to a minor oxidation of Mn(III) to Mn(IV).

Crystals of suitable quality for X-ray diffraction work were selected under an optical microscope. No chemical analysis of the crystals was carried out and their stoichiometry was confirmed as part of their structure determination.

Table 1. Unit-Cell Data for $PbMBO_4$ (Orthorhombic *Pnma* Space Group, $Z = 4$)

M:	Cr[a]	Mn[b]	Fe[b]
a (Å)	6.9501(10)	6.7062(9)	7.0089(14)
b (Å)	5.9410(8)	5.9429(8)	5.9412(12)
c (Å)	8.1386(11)	8.6418(11)	8.3339(17)
volume (Å^3)	336.06	344.41	347.03
r (M^{3+} octahedral, Å)	0.755	0.785	0.785

[a] Powder neutron data. [b] Single-crystal X-ray data.

Structure Determination and Refinement. The crystal structures of $PbFeBO_4$ ($PbMnBO_4$) were determined by single-crystal X-ray diffraction using intensity data collected with a Bruker-AXS diffractometer equipped with a Mo rotating anode generator and a SMART-1K area detector. A total of 8773 (7865) raw intensities were measured and corrected for Lorentz, polarization, and absorption effects using the SAINT[10] and SADABS[11] softwares. The raw data were then averaged to 900 (690) unique reflections and the structures were solved by direct methods and Fourier syntheses using the SHELXL software.[12] The unit-cell data are listed in Table 1. The fully anisotropic refinements converged normally to $wR(F^2)$ indices of 0.062 (0.053) with goodness-of-fit indices of 1.09 (1.21). The final atom coordinates and isotropic displacement parameters are listed in Table 2, and selected bond lengths and angles are listed in Table 3.

The crystal structure of $PbCrBO_4$ was refined by the Rietveld method using both X-ray and neutron powder diffraction data and the $PbGaBO_4$ structure[3] as a starting model. Both refinements led to similar results, although the neutron data yielded smaller esd's (by up to a factor of 10) for the coordinates of the B and O atoms. Accordingly, only the neutron results are included here. The neutron diffraction data were measured at room temperature with the C2 high-resolution diffractometer at the Chalk River Laboratories. Approximately 5 g of $PbCrBO_4$ powder (synthesized from ^{11}B-enriched boric acid as described above) were sealed in a thin-wall vanadium can, and the diffraction pattern was collected over the 5−115° 2θ range (0.1° resolution) using a monochromatized neutron beam ($\lambda = 1.329$ Å). The Rietveld refinement was carried out with the FULLPROF program.[13,14] A relatively short counting time led to a moderate maximum number of counts in the powder diffraction pattern (approximately 700 for a background near 100) which, however, did not preclude the smooth refinement of all atom coordinates and thermal parameters with final reliability indices $R_{wp} = 9.6\%$, $R_{exp} = 8.6\%$, and $\chi^2 = 1.24$. The final atom coordinates and thermal B parameters are listed in Table 2, and selected bond lengths and angles are listed in Table 3.

Magnetic Measurements. Magnetic susceptibility measurements were carried out using a Quantum Design MPMS employing a S.Q.U.I.D. magnetometer at a variety of applied fields over the temperature range 2−350 K.

Powder Neutron Diffraction. Neutron diffraction data were collected using the C2 diffractometer operated by the NRC of Canada through the Neutron Program for Materials

(6) Lavriv, L. V.; Paviikov, V. N.; Lugoskaya, E. S. *Ukr. Khim. Zh.* **1990**, *56*, 455.
(7) Norrestam, R.; Kritikos, M.; Sjödin, A. *J. Solid State Chem.* **1995**, *114*, 311.
(8) Dariet, B.; DeValette, M.; LaTourette, B. *Acta Crystallogr.* **1978**, *B34*, 3528.
(9) LePage, Y.; Calvert, L. D. *Acta Crystallogr.* **1984**, *C40*, 1787.
(10) *SMART and SAINT: Area Detector Control and Integration Software*; Bruker AXS Inc.: Madison, WI.
(11) Sheldrick, G. M. *SADABS: Siemens Area Detector Absorption Correction Software*; University of Göttingen: Göttingen, Germany, 2001.
(12) Sheldrick, G. M. *SHELXL*: *Program for the solution and refinement of crystal structures*; University of Göttingen: Göttingen, Germany, 1997.
(13) Roisnel, T.; Rodriguez-Carvajal, J. *FULLPROF ver 1.9c: Rietveld, Profile Matching & Integrated Intensity Refinement of X-ray and/or Neutron Data*; Laboratoire Léon Brillouin: Saclay, France, 2001.
(14) Roisnel, T.; Rodríguez-Carvajal, J. *WinPLOTR: a Windows tool for powder diffraction patterns analysis*, Materials Science Forum, Proceedings of the Seventh European Powder Diffraction Conference (EPDIC 7); Delhez, R., Mittenmeijer, E. J., Eds.; Transtech Publications: Zurich, Switzerland, 2000; pp 118−123.

Table 2.

(A) Atomic Coordinates and Isotropic Displacement Parameters of $PbMBO_4$

	x	*y*	*z*	B^a (Å²)
Pb	0.0599(8)	0.25	0.3650(7)	0.34(10)
Cr	0	0	0	0.66(24)
B	−0.2247(11)	0.25	−0.2666(9)	0.16(14)
O1	0.1075(13)	−0.25	−0.1231(12)	0.40(16)
O2	0.1725(9)	−0.0477(11)	0.1919(7)	0.20(12)
O3	−0.1670(13)	−0.25	0.0930(11)	0.66(15)

	x	*y*	*z*	$U_{eq}{}^b$ (Å²)
Pb	0.03542(4)	0.25	0.35174(3)	0.0126(1)
Mn	0	0	0	0.0082(2)
B	−0.2089(9)	0.25	−0.2611(8)	0.010(1)
O1	0.1090(7)	−0.25	−0.1043(6)	0.0101(7)
O2	0.1681(5)	−0.0463(5)	0.1871(4)	0.0128(6)
O3	−0.2160(8)	−0.25	0.0929(6)	0.0133(8)

	x	*y*	*z*	$U_{eq}{}^b$ (Å²)
Pb	0.05624(4)	0.25	0.35702(3)	0.0105(1)
Fe	0	0	0	0.0040(2)
B	−0.2200(11)	0.25	−0.2657(9)	0.009(1)
O1	0.1071(8)	−0.25	−0.1155(6)	0.0077(8)
O2	0.1697(6)	−0.0494(6)	0.1950(4)	0.0122(7)
O3	−0.1820(8)	−0.25	0.0894(6)	0.0107(9)

(B) Anisotropic Displacement Parameters (Å²) for $PbMBO_4$ (M = Mn, Fe)

	U_{11}	U_{22}	U_{33}	U_{23}	U_{13}	U_{12}
Pb	0.0137(2)	0.0160(2)	0.0081(2)	0	0.00054(7)	0
Mn	0.0088(3)	0.0081(3)	0.0077(4)	−0.009(3)	−0.0011(3)	0.0009(3)
B	0.006(3)	0.013(2)	0.010(3)	0	0.001(2)	0
O1	0.009(2)	0.011(2)	0.011(2)	0	0.001(2)	0
O2	0.017(1)	0.010(1)	0.011(1)	0.000(1)	−0.005(1)	0.001(1)
O3	0.014(2)	0.015(2)	0.011(2)	0	0.004(1)	0

	U_{11}	U_{22}	U_{33}	U_{23}	U_{13}	U_{12}
Pb	0.0116(1)	0.0132(1)	0.0067(1)	0	0.00081(8)	0
Fe	0.0058(4)	0.0029(3)	0.0033(3)	−0.0009(3)	−0.0009(3)	0.0008(3)
B	0.011(3)	0.009(3)	0.007(3)	0	−0.001(2)	0
O1	0.008(2)	0.008(2)	0.007(2)	0	−0.002(2)	0
O2	0.016(1)	0.009(1)	0.010(1)	0.000(1)	−0.006(1)	0.003(1)
O3	0.014(2)	0.010(2)	0.008(2)	0	0.006(2)	0

[a] Powder neutron diffraction data. [b] Single-crystal X-ray diffraction data.

Table 3. Selected Bond Distances (*l*, Å), Bond Valences (*s*), and Bond Angles (deg) in $PbMBO_4$

	$PbCrBO_4$		$PbMnBO_4$		$PbFeBO_4$	
	l	*s*	*l*	*s*	*l*	*s*
Pb−O1	2.287(11)	0.62	2.347(5)	0.53	2.316(6)	0.58
Pb−O1	2.313(10)	0.59	2.414(5)	0.44	2.370(6)	0.50
Pb−O2 ×2	2.393(7)	0.47	2.433(3)	0.42	2.370(4)	0.50
Σ*s* (Pb)		2.15		1.79		2.08
M−O1 ×2	1.941(6)	0.56	1.885(3)	0.71	1.923(3)	0.64
M−O2 ×2	1.989(6)	0.49	1.990(3)	0.54	2.035(4)	0.47
M−O3 ×2	2.031(6)	0.44	2.225(4)	0.28	2.095(4)	0.40
Σ*s* (M)		2.98		3.06		3.02
B−O2 ×2	1.395(7)	0.94	1.396(5)	0.93	1.376(5)	0.99
B−O3	1.369(12)	1.00	1.358(8)	1.04	1.389(9)	0.95
Σ*s* (B)		2.88		3.00		2.93
Σ*s* (O1)		2.33		2.40		2.36
Σ*s* (O2)		1.90		1.89		1.96
Σ*s* (O3)		1.88		1.61		1.76
O1−M−O2	93.6(5)		93.5(2)		93.4(2)	
O1−M−O2	86.3(4)		86.6(2)		86.6(2)	
O1−M−O3	81.5(6)		84.2(1)		82.4(1)	
O1−M−O3	98.5(3)		95.8(1)		97.6(2)	
O2−M−O3	87.0(5)		89.0(2)		88.3(2)	
O2−M−O3	93.0(5)		91.0(2)		91.8(2)	
O2−B−O2	119.0(7)		120.2(5)		120.1(6)	
O2−B−O3	120.5(9)		119.9(3)		119.9(3)	
M−O1−M	99.8(3)		104.0(2)		101.2(2)	
M−O3−M	94.0(3)		83.8(2)		90.2(2)	

Research. Samples of 2−4 g were contained in thin-walled vanadium sample cans sealed under argon gas with an indium gasket. Neutrons of wavelength $\lambda = 2.3707$ or 1.3287 Å were obtained from a Ge monochromator. Samples were cooled using a standard Orange cryostat to a minimum temperature of 2 K. Temperature control was ±0.1 K. Rietveld refinements were done using FULLPROF in the WINPLOTR format.[14]

Results and Discussion

Description of the $PbMBO_4$ Structure. The $PbMBO_4$ compounds (M = Cr, Fe, Mn) crystallize with a novel structure type previously unknown among anhydrous borates.[15,16] The only other members of this structural family are $PbGaBO_4$[3] and the low-temperature polymorph of $PbAlBO_4$.[4] Efforts to extend the crystal chemistry of this structure type to other trivalent ions, such as Ti, V, Co, Sc, Y, and In, were unsuccessful for a variety of reasons. For Ti and V, internal redox thermodynamics results in reduction of Pb^{2+} to Pb metal and oxidation of the transition metal; for Co, the trivalent oxidation state cannot be stabilized in 1 atm of oxygen; and for Sc, Y, and In, the M^{3+} cations are all too large for this structure type.

As illustrated in Figure 1, the $PbMBO_4$ structure is built of single [010] chains of edge-shared MO_6 octahedra bridged by orthoborate BO_3 groups forming a three-dimensional MBO_4^{2-} framework. The Pb^{2+} cations occupy unsymmetrical 4-fold coordination sites typical of their stereoactive lone pairs and fill the empty [010] tunnels within the MBO_4^{2-} framework. The linear isolated octahedral chains provide a strong one-dimensional character to the structure, which is apparent in the magnetic properties of the $PbMBO_4$ compounds (see below).

(15) Heller, G. *Top. Curr. Chem.* **1986**, *131*, 39.
(16) Grice, J. D.; Burns, P. C.; Hawthorne F. C. *Can. Miner.* **1999**, *37*, 731.

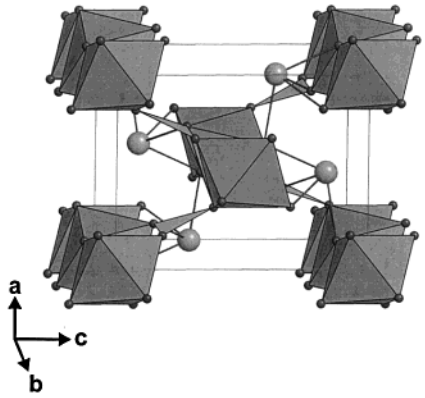

Figure 1. View of the $PbMnBO_4$ structure showing [010] chains of edge-sharing MnO_6 octahedra bridged by BO_3 groups and Pb^{2+} cations (spheres) in asymmetric 4-fold coordination sites.

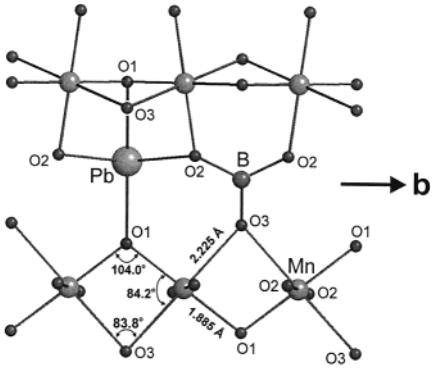

Figure 2. View of two adjacent [010] octahedral chains in the $PbMnBO_4$ structure showing the asymmetric Mn−O−Mn linkages.

An interesting feature of the $PbMBO_4$ structure is the distorted octahedral coordination of the M^{3+} cations. Although the bond-valence sums around the cations are close to their expected values in all structures, a rather wide range of M−O distances is observed, including short M−O1 and long M−O3 bonds (Table 3). This difference in M−O bond lengths is consistent with the bond topology of the structure and the different coordination environments of the O1 (2Pb + 2M) and O3 (2M + B) atoms: without a large valence contribution from strong bonds to boron, the O1 atom requires stronger, that is, shorter, bonds to M to maintain a proper bond-valence sum. It is noteworthy, however, that the O1 atom remains over-bonded ($\Sigma s \approx 2.40$) and the O3 atom under-bonded ($\Sigma s = 1.60-1.88$) in all structures. Such deviations in bond-valence sums suggest the presence of structural strain in the $PbMBO_4$ structures, which can be associated with the strong tilting along the [010] octahedral chains caused by the bridging BO_3 groups (Figure 2). The BO_3 groups indeed impose a strong geometrical constraint on the unit cell as shown by the nearly constant value of the *b* parameter in the $PbMBO_4$ series (Table 1). This constraint also implies a limiting size for the MO_6 octahedra and accounts for the impossibility to synthesize a $PbMBO_4$ phase for M = Sc, Y, or In. These compounds might, however, form under high-pressure conditions based on the higher compressibility expected for the M−O bonds relative to that of the B−O bonds. As expected, the Jahn−Teller effect associated with the $3d^4$ Mn^{3+} cation

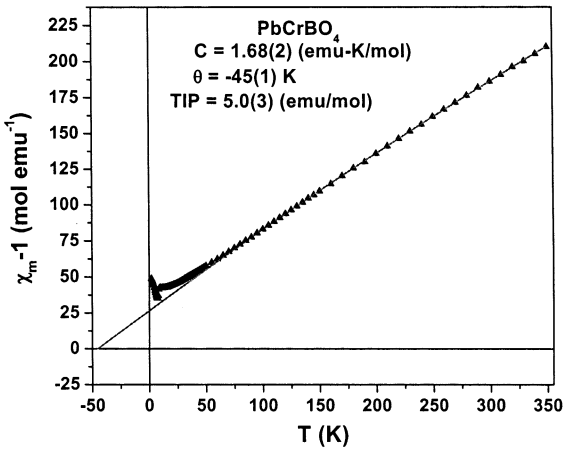

Figure 3. Inverse susceptibility for $PbCrBO_4$. The fit is to a modified Curie−Weiss law with $C = 1.68(2)$ emu·K/mol, $\theta_c = -45(1)$ K, and TIP $= 5.0(3) \times 10^{-4}$ emu/mol.

leads to the largest octahedral distortion in $PbMnBO_4$ (Table 3). This effect is reflected in irregular *a* and *c* unit-cell parameters and in significant shifts of atomic positions in the $PbMnBO_4$ structure (Tables 1 and 2). It is of course the edge-sharing [010] octahedral chains which are the most important feature for the magnetic properties. While similar octahedral chains are found in a limited number of other oxide structure types, most notably the rutile structure, there are two aspects of the chains in $PbMBO_4$ which appear to be unique. First, the shortest interchain separation is ~5.5 Å, sufficiently long to promote some one-dimensional character. As well, the interchain linkages are via the BO_3 and PbO_4 groups as seen in Figure 2, and the superexchange pathways are rather convoluted. By contrast, the octahedral chains in the rutile structure are connected directly by corner sharing. Second, the M−O−M edge-sharing bridging angles in $PbMBO_4$ are highly asymmetric, with differences ranging from 6° (M = Cr) to 20° (M = Mn) (Table 3). In rutile and related structures the bridging angles are symmetric.

Magnetic Measurements and Magnetic Structures. *$PbCrBO_4$.* Susceptibility data are shown in Figures 3 and 4 for the temperature range 2−350 K. The inverse susceptibility data, Figure 3, can be fitted over the temperature range 100−350 K to a modified Curie−Weiss law yielding fitting constants $C = 1.68(2)$ emu·K/mol, $\theta = -45(1)$ K, and a temperature-independent term, (TIP) $= 5.0(3) \times 10^{-4}$ emu/mol. The Curie constant is close to the expected spin-only value of 1.87 emu·K/mol for a $S = {}^3/_2$ ion and the negative Weiss temperature indicates net antiferromagnetic exchange. Two features are evident in Figure 4, (inset), a sharp maximum near 8 K showing a marked divergence between the zero-field-cooled (ZFC) and field-cooled (FC) data and a broad maximum centered near 13 K. It is reasonable to assign the broad maximum to short-range one-dimensional correlations (SRO) and the sharp feature to long-range antiferromagnetic order (LRO) with probable spin canting. A fit to a $S = {}^3/_2$ linear chain model is shown in Figure 4.[17,18] The agreement is

(17) Weng, C. Y. Ph.D. Thesis, Carnegie Mellon University, Pittsburgh, PA, 1969.

(18) Hiller, W.; Strahle, J.; Datz, A.; Hanack, M.; Hatfield, W. E.; Ter Haar, L. W.; Gutlich, P. *J. Am. Chem. Soc.* **1984**, *106*, 329.

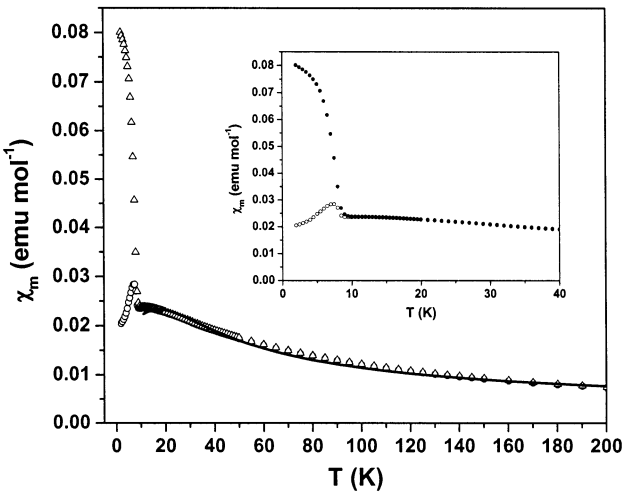

Figure 4. Fit (solid line) of the 1D $S = {}^3/_2$ model[17,18] to the susceptibility for $PbCrBO_4$. The inset shows the low-temperature susceptibility. The open circles are the zero-field-cooled (ZFC) data and the filled circles are the field-cooled (FC) data.

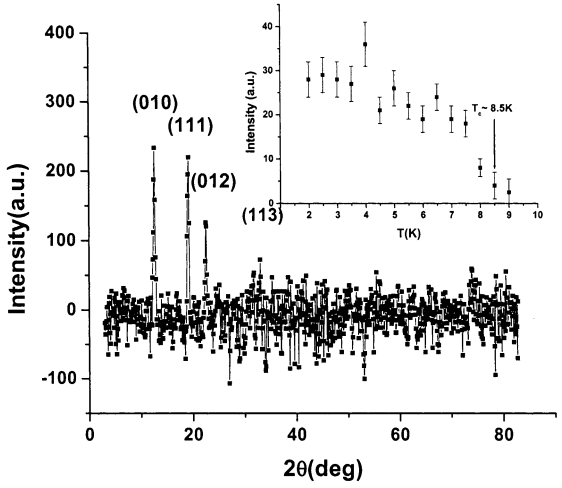

Figure 5. Difference intensity data for $PbCrBO_4$ obtained by subtracting the 9.5 K data from the 2 K data (neutron wavelength = 1.3287 Å). The difference peaks are indexed on the chemical cell. The inset shows the temperature dependence of the (111) magnetic reflection consistent with $T_c = 8.5$ K.

reasonable except for the rather large *g*-factor of 2.57. This is likely due to the proximity of the SRO and LRO features, particularly as the LRO ground state appears to involve canted spins and, thus, a net moment. The intrachain exchange constant, $J^{intra}/k_B = -3.7$ K. This is a slightly larger value than one finds from the position of $T(\chi_{max}) \sim 13$ K and the numerical results of Weng[17] as tabulated by de Jongh and Miedema,[20] $k_B T(\chi_{max})/J^{intra} \cong 4.75$, which gives $J^{intra}/k_B = -2.7$ K. Again, this discrepancy is likely due to the proximity of the broad and sharp susceptibility maxima for this compound.

Neutron diffraction patterns were obtained over the temperature range 2−10 K. A plot of the intensity difference between patterns obtained at 2 K and at 9.5 K is displayed in Figure 5. New, resolution-limited, Bragg reflections appear in the 2 K data set, the most prominent ones with indices (010), (111), (012), and (113), which indicate the presence of long-range antiferromagnetic order with an ordering wavevector, **k** = (000). The (010) and (012) reflections are forbidden in the chemical cell space group, *Pnma*. The temperature dependence of the intensity of the (111) magnetic reflection is shown in Figure 5 (inset) and a $T_c \sim 8.5$ K can be estimated, in good agreement with the susceptibility maximum.

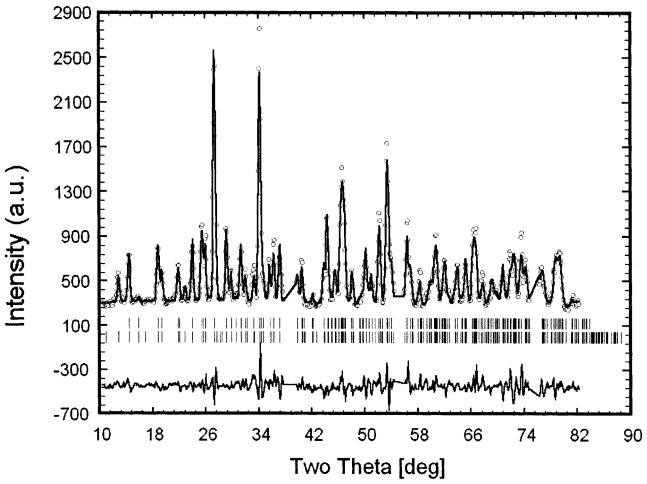

Figure 6. Refinement of the crystal and magnetic structures for $PbCrBO_4$ at 2 K. The open circles are the data, the solid line is the fit, and the bottom line is the difference plot. The upper set of tic marks locates the crystal structure Bragg peaks and the lower set the magnetic Bragg peaks.

Table 4. Results of Magnetic Structure Refinements for $PbMBO_4$, M = Cr, Fe, Mn

	Cr	Mn	Fe
T (K)	2.0	4.3	10.0
a (Å)	6.946(1)	6.7020(8)	6.984(1)
b (Å)	5.915(1)	5.9226(7)	5.974(1)
c (Å)	8.118(1)	8.577(1)	8.345(2)
Pb(*x*,*z*)	0.0598(1)	0.0402(1)	0.0562(3)
	0.3635(7)	0.3519(6)	0.3570(6)
B(*x*,*z*)	−0.225(1)	−0.206(1)	−0.220(1)
	−0.267(1)	−0.261(1)	−0.256(1)
O1(*x*,*z*)	0.107(2)	0.111(1)	0.107(1)
	−0.121(1)	−0.103(1)	−0.116(1)
O2(*x*,*y*,*z*)	0.1660(9)	0.1679(10)	0.1697(11)
	−0.0451(1)	−0.0464(1)	−0.0494(1)
	0.1943(8)	0.1879(7)	0.1950(9)
O3(*x*,*z*)	−0.1680(15)	−0.2133(13)	−0.1820(11)
	0.0937(12)	0.0927(10)	0.0894(10)
B(Å^2)	0.3(2)	1.0(1)	2.9(8)
$\mu(M^{3+}/\mu_B)$	2.02(7) (*x*)	3.9(1) (*x*)	4.05(7) (*z*)
χ^2	3.98	3.77	4.07
R_{Bragg} (%)	6.32	7.48	10.2
R_{MAG} (%)	17.0	8.02	5.7

The magnetic structure could be refined from the neutron data, Figure 6. The model which best fits the data has the Cr^{3+} moments aligned antiparallel along the *b*-axis (chain axis) with a preferred direction along *a* and the moments in the *ac* planes forming ferromagnetic sheets; that is, the chains are coupled ferromagnetically. This magnetic structure is indeed incompatible with the n-glide symmetry of the chemical cell space group, *Pnma*. Other models with the preferred moment direction along *c* or in the *ac* plane gave significantly poorer results. Models with (AF) interchain coupling result in magnetic reflections with indices different from those observed. The refined Cr^{3+} moment is 2.02(7) μ_B, much smaller than the 3.0 μ_B expected from a $S = {}^3/_2$ ion. This is a common result for low-dimensional systems. The full refinement results are displayed in Table 4. The slightly larger than usual agreement indices are due to contamination of the diffraction pattern by weak reflections from the cryostat.

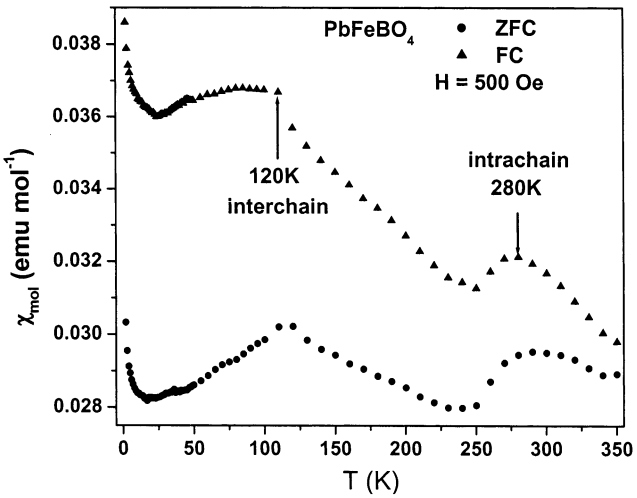

Figure 7. Susceptibility of $PbFeBO_4$ showing maxima due to both interchain and intrachain correlations. The circles are the ZFC data and the triangles are the FC data.

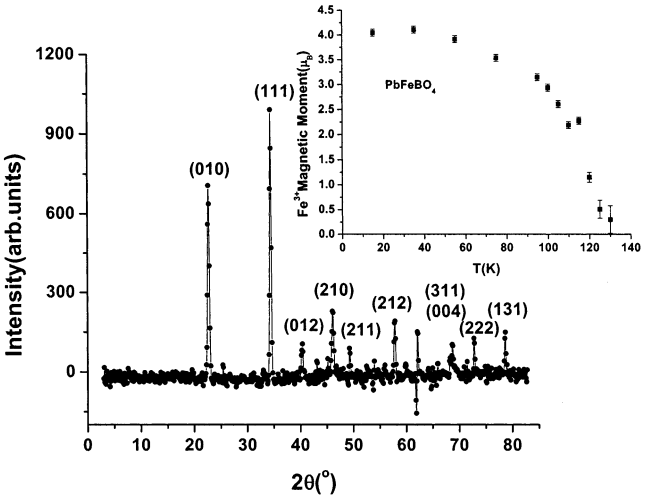

Figure 8. Intensity difference for $PbFeBO_4$ obtained by subtracting the data at 135 K from data at 15 K (neutron wavelength = 2.3707 Å). The magnetic Bragg peaks are indexed on the chemical cell. The inset shows the temperature dependence of the ordered Fe^{3+} magnetic moment, consistent with $T_c = 125$ K.

$PbFeBO_4$. The temperature dependence of the magnetic susceptibility for this compound is shown in Figure 7. Note the presence of two maxima over the temperature range studied and that the FC and ZFC curves diverge even at 350 K. This latter behavior can be traced to the presence of ~5 wt % of α-Fe_2O_3, which orders in a helical magnetic structure with a net moment at 950 K.[19] The broad maximum centered near 280 K can be attributed to one-dimensional, antiferromagnetic (AF) SRO and the sharper feature at ~120 K to AF LRO, to be confirmed by neutron scattering experiments. Thus, in this material the one-dimensional feature is well-separated from that signaling the AF LRO, in contrast to the Cr analogue just discussed. Unfortunately, the presence of the α-Fe_2O_3 contaminant renders any quantitative fitting of the susceptibility data impossible but one can obtain an estimate of J^{intra}/k_B from the position of χ_{max} and the numerical results of Weng,[17,18] tabulated by de Jongh and Miedema.[20] That is, for a $S = {}^5/_2$ 1d AF system $k_B T(\chi_{max})/J^{intra} \cong 10.6$ and, thus, for $PbFeBO_4 = -26$ K. This is nearly 10 times greater than the corresponding value for $PbCrBO_4$.

The result of subtracting neutron diffraction data sets obtained at 135 and 15 K is shown in Figure 8. Several strong difference peaks are seen which, as in the case of $PbCrBO_4$, can be indexed on the chemical unit cell; that is, the ordering wave vector is $k = (000)$, and the indices are also the same, suggesting a similar magnetic structure.

The inset shows the temperature dependence of the refined Fe^{3+} moment and confirms that $T_c = 125$ K. The magnetic structure was solved and the Rietveld refinement result for 15 K is shown in Figure 9 (TOP). The 5 wt % α-Fe_2O_3 contaminant was included in the refinement of the chemical structure but not in that of the magnetic structure since the magnetic reflections for α-Fe_2O_3 do not overlap those for $PbFeBO_4$. In view of these complications, the agreement indices are satisfactory. Final refinement results are displayed in Table 4. The magnetic structure (bottom) is indeed similar to that for $PbCrBO_4$, with ferromagnetic sheets of spins in the *ac* plane coupled antiferromagnetically along the *b* or chain axis, but with the preferred moment direction now along the *c* axis. The ordered moment for Fe^{3+} is 4.05(8) μ_B at 15 K, again much reduced from the expected spin-only value of 5 μ_B for a $S = {}^5/_2$ ion.

$PbMnBO_4$. This material differs from the Cr and Fe analogues in nearly all respects. First, the susceptibility data, Figure 10, are consistent with overall ferromagnetic behavior, showing a sharp rise just below about 30 K. The inset shows a plot of the Fisher heat capacity ($d\chi T/dT$ vs T) indicating a $T_c = 31$ K.[21] The inverse susceptibility data, Figure 11, can be fitted to a modified Curie–Weiss law again, with fitting parameters $C = 3.04(2)$ emu·K/mol, $\theta_c = +52.5(7)$ K, and a TIP term = 1.67×10^{-3} emu/mol. The Curie constant is essentially that expected for spin-only Mn^{3+}, a $S = 2$ ion, 3.00 emu·K/mol. The Weiss temperature is now fairly large and positive, indicating overall ferromagnetic exchange. The TIP term is surprisingly large, and the data show curvature throughout the temperature range investigated, showing that a pure Curie–Weiss regime is not obtained. Thus, one should regard the fitting results just presented with a certain level of skepticism but the Curie constant or effective moment is compellingly close to the expected value and the positive Weiss temperature is consistent with ferromagnetism, which is observed. Examination of the data above T_c indicate, Figure 12, that the short-range correlations are ferromagnetic, as evidenced by the positive divergence of the magnetic moment (χT) with decreasing temperature. These data were fitted to Fisher's expression for a linear chain, ferromagnetic, classical spin model by scaling to $S = 2$,[22] as shown in the inset. The extracted parameters are $J^{intra}/k_B = 11(3)$ K and $g = 1.8(3)$.

Neutron diffraction data in the form a difference plot, 4.3–33.5 K, Figure 13 (left), show many strong, residual reflections with very different indices than those for the

(19) Tasaki, A.; Shiratori, K.; Iida, S. *J. Phys. Soc. Jpn.* **1962**, *17B-1*, 235.
(20) De Jong, L. J.; Miedema, A. R. *Adv. Phys.* **1974**, *23*, 34.
(21) Fisher, M. E. *Philos. Mag.* **1962**, *7*, 1731.
(22) Fisher, M. E. *Am. J. Phys.* **1964**, *32*, 343.

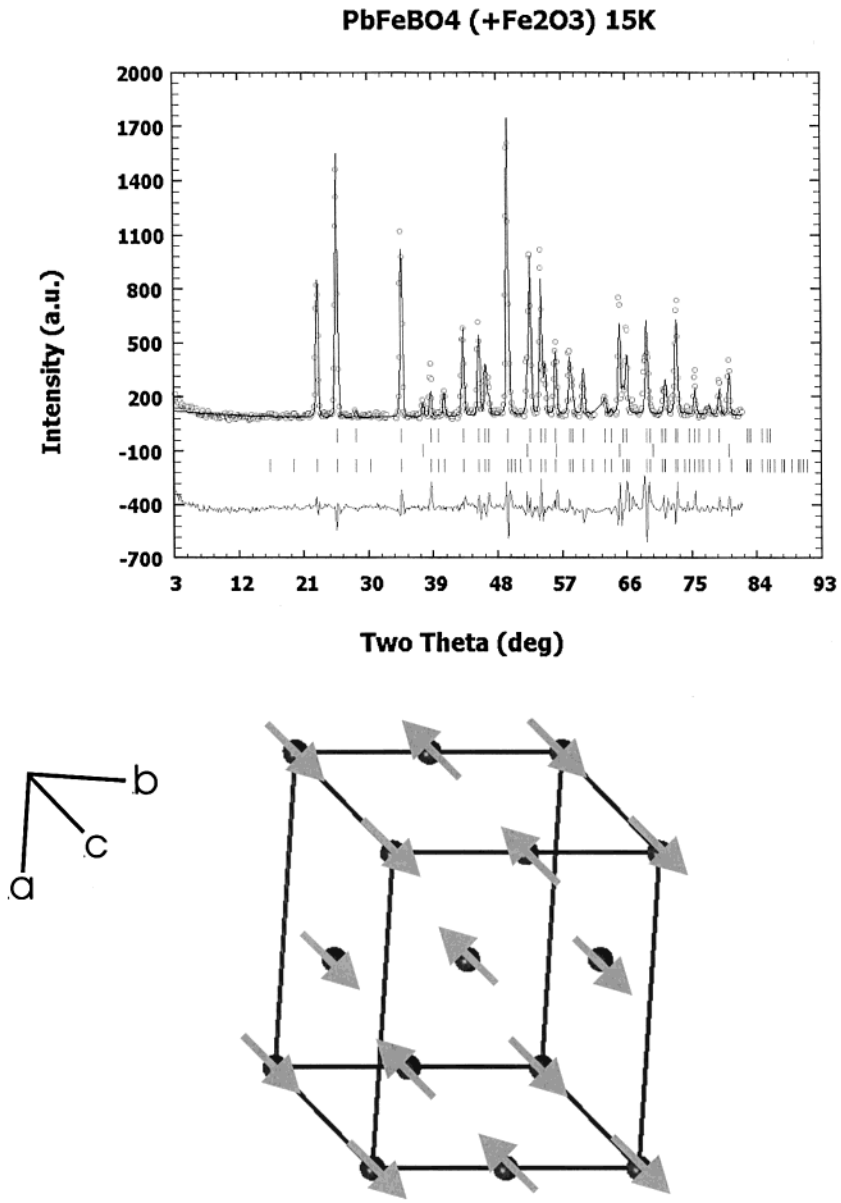

Figure 9. Top: Refinement of the crystal and magnetic structures of $PbFeBO_4$. The open circles are the data, the solid line is the fit, and the bottom line is the difference plot. The top and bottom sets of tic marks locate the Bragg peak positions for the crystal and magnetic structures, respectively, and the middle set is for the crystal structure of α-Fe_2O_3. Bottom: The magnetic structure of $PbFeBO_4$.

antiferromagnetic materials but still with $\mathbf{k} = (000)$. The magnetic structure was solved on a ferromagnetic model with the preferred moment direction along the *a* axis. The refinement results are tabulated in Table 4. In this case the ordered moment is 3.91(1) μ_B, very close to the 4.0 μ_B expected for an $S = 2$ ion. The temperature dependence of the intensity of the (101) reflection, Figure 13 (right), yields a $T_c = 31$ K, in excellent agreement with the Fisher's heat capacity analysis, Figure 10.

Thus, the magnetic properties of the three isostructural $PbMBO_4$ materials studied here show surprising variation. The M = Cr and Fe phases exhibit both one-dimensional AF SRO and AF LRO. In both cases the interchain exchange coupling appears to be ferromagnetic, as evidenced by the magnetic structure. In sharp contrast the M = Mn material displays one-dimensional F SRO and F LRO. The Mn compound is remarkable as it is a new ferromagnetic insulator (single crystals are dark red and transparent). Ferromagnetic insulators are among the rarest of magnetic materials. Among oxides, there are only a few other examples, such as EuO, $YTiO_3$, $Lu_2V_2O_7$, and VBO_3, with T_c's substantially above 4 K.[23−26]

Table 5 collects the measured J^{intra}/k_B values for the three materials studied. Note first that the sign and magnitude of J^{intra}/k_B is a surprisingly strong function of the electronic configuration, given here in the pseudo-octahedral representation. Perhaps, most surprising, is the large value for the ferromagnetic intrachain cou-

(23) Matthias, B. T.; Bozorth R. M.; van Vleck, J. H. *Phys. Rev. Lett.* **1961**, *7*, 160.
(24) Greedan, J. E.; MacLean, D. A. *Inst. Phys. Conf. Ser.* **1978**, *37*, 249.
(25) Bazuev, G. V.; Makarova, O. V.; Oboldin, V. Z.; Shveikin, G. P. *Dokl. Akad. Nauk SSSR* **1976**, *230*, 869. Soderholm, L.; Greedan, J. E. *Mater. Res. Bull.* **1979**, *14*, 1449.
(26) Bither, T. A.; Frederick, C. G.; Gier, T. E.; Weiher, J. F.; Young, H. S. *Solid State Commun.* **1970**, *8*, 109.

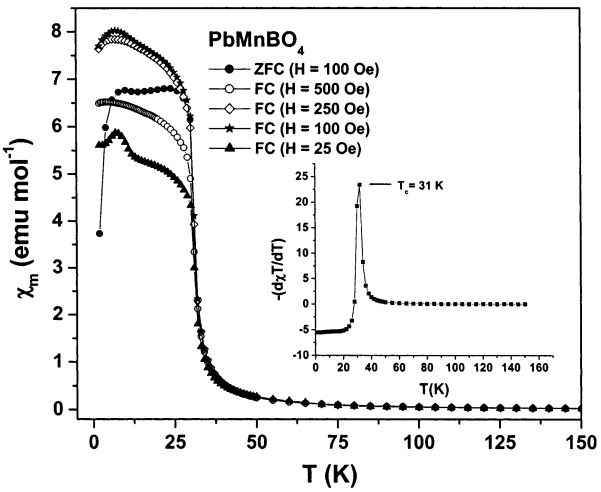

Figure 10. The susceptibility of $PbMnBO_4$ at a variety of fields and conditions. The inset shows the Fisher's heat capacity[21] ($d\chi T/dt$ vs T), indicating a ferromagnetic $T_c = 31$ K.

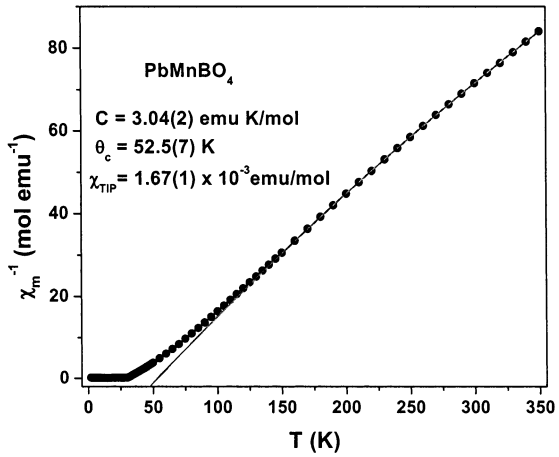

Figure 11. Fit of the modified Curie−Weiss law for $PbMnBO_4$. The fitting parameters are $C = 3.04(2)$ emu·K/mol, $\theta_c = 52.5(7)$ K, and TIP $= 1.67 \times 10^{-3}$ emu/mol.

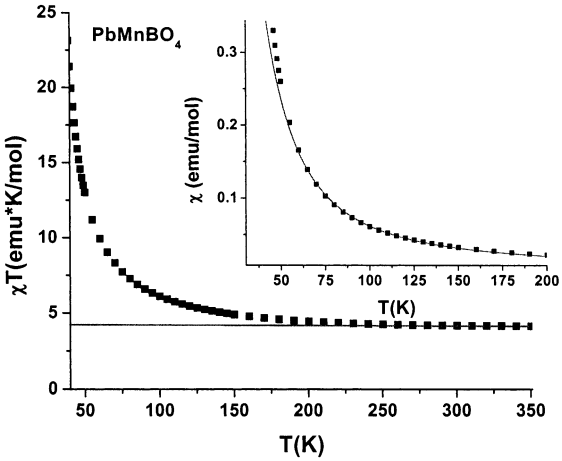

Figure 12. Evidence for 1D ferromagnetic correlations in $PbMnBO_4$. The inset shows a fit to Fisher's model for a 1D ferromagnetic scaled to $S = 2$.[22]

pling for the Mn compound; it is >2 times the magnitude for $PbCrBO_4$ and $^1/_2$ that for $PbFeBO_4$. In insulators, ferromagnetic exchange constants are normally weaker, often by an order of magnitude, compared with those for antiferromagnetic exchange in isostructural systems.

Table 5. Measured J^{Intra} Values for the $PbMBO_4$ Series

M^{3+}	electron config.	J^{intra}/k_B (K)
Cr	$t_2^3\ e^0$	−4
Mn	$t_2^3\ e^1$	+11
Fe	$t_2^3\ e^2$	−26

As already mentioned, the $PbMBO_4$ materials present a new structure type and the presence of relatively well isolated chains of edge-sharing octahedra is a feature not found in other magnetic oxides and, thus, no direct comparisons can be made. There is, nonetheless, a reasonable amount of literature on dimeric compounds in which the primary nearest neighbor M−M environment consists of edge-sharing octahedra which may provide a context for the systematics exhibited in Table 5.

Beginning with the Cr phase, it is important to recognize that exchange between two d^3 ions for a ∼90° geometry is the resultant of contributions from many pathways. Direct $t_{2g}-t_{2g}$ interactions as well as both σ and π symmetry Cr−O−Cr superexchange must usually be considered.[27] In the absence of detailed calculations, one can search for magnetostructural correlations. The most relevant studies are probably those on the trirutile oxides, Cr_2WO_6 and Cr_2TeO_6, along with the related compound, $Cr_2Te_4O_{11}$, all of which contain $Cr_2O_{10}^{14-}$ edge-sharing octahedral dimers, although in these materials the bridging angles are symmetric.[28,29] It was shown that J^{dimer}/k could be correlated well with either the bridging angle or the Cr−Cr distance, values for which range from −45 K at 97.9° and 2.94 Å (Cr_2WO_4) to −33 K at 98.7° and 2.98 Å (Cr_2TeO_6) to −4.2 K at 101.2° and 3.019 Å ($Cr_2Te_4O_{11}$).[28,29] Clearly, the value of J^{intra}/k_B for the $PbCrBO_4$ material is at the low end of known values for oxide ligand compounds. The average intrachain bridging angle for $PbCrBO_4$ is 96.9°, although the asymmetry is significant (99.8(3)° and 94.0(3)°). It is not clear that the mean value is a useful parameter here and, in any case, it lies outside the range of angles covered by the trirutile series. The Cr−Cr distance in $PbCrBO_4$ is 2.97 Å (b/2).

On the basis of the distance correlation, one would expect $J/k_B \sim -38$ K, a much more negative value than observed. Other compounds which might be relevant here are di-oxo bridged, that is, edge-sharing, molecular dimers of the type $[L_4Cr-O]_2^{2+}$. Unfortunately, while there exists a substantial amount of literature for hydroxo-bridged dimers,[30] very few examples of the di-oxo species have been synthesized and characterized. One known example is the complex $[(2\text{-picetam})_2CrO]_2Cl_2\cdot 8H_2O$ for which $J/k = -58$ K was found, although the crystallographic details were not reported.[31] Thus, the observed $J^{intrachain}$ is anomalously low for $PbCrBO_4$, and in the absence of better model systems for comparison or detailed calculations, this fact remains unexplained.

For the case of $PbFeBO_4$ only two relevant oxides have been studied, the trirutile Fe_2TeO_6 (Fe_2WO_4 has

(27) Martin, R.L. In *New Pathways in Inorganic Chemistry*; Cambridge University Press: Cambridge, 1968; Chapter 9, p 208.
(28) Drillon, M.; Padel, L.; Bernier, J. C. *J. Chem. Soc., Faraday 2* **1980**, *76*, 1224. Charlot, M. F., Khan, O.; Drillon, M. *Chem. Phys.* **1982**, *70*, 177.
(29) Khan, O.; Briat, B.; Galy, J. *J. Chem. Soc. Dalton* **1977**, 1453.
(30) Hatfield, W. E.; MacDougal, J. J.; Shepherd, R. E. *Inorg. Chem.* **1981**, *20*, 4216.
(31) Michelsen, K.; Pedersen, E.; Wilson, S. R.; Hodgson, D. J. *Inorg. Chim. Acta* **1982**, *63*, 141.

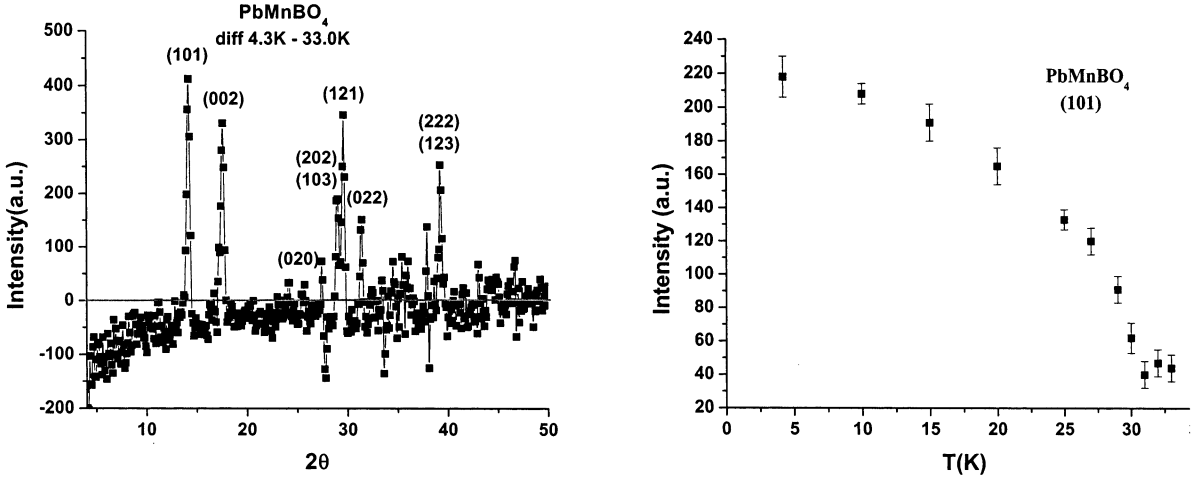

Figure 13. Left: The intensity difference plot for $PbMnBO_4$ obtained by subtracting data at 33.0 K from data at 4.3 K (neutron wavelength = 1.3287 Å). The magnetic Bragg peaks are indexed on the chemical cell. Right: The temperature dependence of the intensity of the (101) magnetic reflection, consistent with $T_c = 31$ K.

the α-PbO_2 structure with no isolated dimers)[32] and $Fe_2Te_4O_{11}$ which does contain edge-shared dimers but is not precisely isostructural with $Cr_2Te_4O_{11}$.[33] For the trirutile phase, susceptibility data show a broad maximum at ∼240 K but no detailed fit has been done. With use of the relationship for $S = {}^5/_2$ dimers, $k_BT(\chi_{max})/J^{dimer} = 5.761$,[27] a value of −42 K can be estimated. Relevant geometric parameters for this material include a unique Fe−O−Fe angle of 98.3° and an Fe−Fe intradimer distance of 3.026 Å. $Fe_2Te_4O_{11}$ also contains well-isolated dimers but the Fe−O−Fe angles are quite asymmetric with values of 110° and 91° (average 100.5°) and the Fe−Fe separation is 3.35 Å. Here, the susceptibility maximum occurs at 39 K, which translates to $J^{intrachain}/k_B = -6.8$ K. The same trend as for the Cr case is seen; intradimer exchange decreases with increasing Fe−O−Fe angle and Fe−Fe distance. The corresponding angles and distances of $PbFeBO_4$ lie below these limits, with an Fe−O−Fe average angle of 95.5° and an Fe−Fe intradimer distance of 2.97 Å. Assuming a linear correlation of J/k_B with both parameters, one would then expect a relatively large, negative intrachain exchange of ca. −120 K (angle) to −50 K (distance), both being significantly more negative than the observed value of −26 K. Again, the number of well-characterized molecular dimers with di-oxo bridges is limited. The complex $[Fe_2(\mu\text{-}O)_2(6TLA)_2](ClO_4)_2$ has an Fe−Fe distance of only 2.714(2) Å and an Fe−O−Fe angle of 92.5° and shows a $J/k = -38$ K, but the Fe_2O_2 core geometry is far from that of $PbFeBO_4$.[34] As with the case of $PbCrBO_4$, the observed J/k_B appears to be anomalously low.

Finally, for $PbMnBO_4$ the most relevant comparison is with Mn_2TeO_6, which exists in the trirutile structure with a Mn−Mn separation of 3.02 Å and an Mn−O−Mn angle of 99.9°, but the susceptibility data have not been published.[35] This one report comments on the absence of a broad maximum above the long-range ordering temperature of $T_c = 25.5$ K and notes that the observed magnetic structure, while antiferromagnetic, is non-collinear and much more complex than that usually found for trirutile oxides such as Fe_2TeO_6 and Cr_2TeO_6. It was suggested that competition between intradimer ferromagnetic and interdimer antiferromagnetic exchange could be responsible for the non-collinear magnetic structure but the magnitude of the exchange constants could not be determined. Another possibly relevant oxide is $LiMnO_2$. In this material, puckered layers of edge-sharing MnO_6 octahedra exist with two geometries. Along the shortest axis (*a* in this case) Mn chains exist with a separation of 2.806(1) Å and Mn−O−Mn angles of 95.6 and 89.7°.[36] The interchain Mn−Mn distance is 3.15 Å and the Mn−O−Mn angle is 94.2°. The Curie−Weiss θ_c equals −1056(13) K, which suggests that the in-plane exchange interactions are strongly antiferromagnetic. A well-characterized di-oxo bridged molecular dimer does exist in the form of $[Mn(6Me_2\text{-bispicen})_2O]_2^{2+}$ where the Mn−Mn distance is 2.676 Å, the Mn−O−Mn angle is 93.9°, and $J/k = -120$ K.[37] This is a considerably shorter Mn−Mn distance than for $PbMnBO_4$ and the other oxides but the angle matches very well the average (93.9°). Calculated *J* values for planar, di-oxo bridged dimers tend to be large and antiferromagnetic.[38] It is clear from the above information that the ferromagnetic intrachain *J* for $PbMnBO_4$ would not be expected, although no truly comparable model system exists and calculations have not been done for the observed Mn_2O_2 core geometry.

Summary and Conclusions

The crystal chemistry of a new structure type in the Pb−M−B−O system, $PbMBO_4$, has been investigated. Among the transition elements, the only stable phases

(32) Dehn, J. T.; Newnham, R. E.; Mulay, L. N. *J. Chem. Phys.* **1968**, *49*, 3201. Kunnmann, W.; La Placa, S.; Corliss, L. M.; Hastings, J. M.; Banks, E. *J. Phys. Chem. Solids* **1968**, *29*, 1359. Yamaguchi, M.; Ishikawa, M. *J. Phys. Soc. Jpn.* **1994**, *63*, 1666.

(33) Jumas, J. C.; Fournes, L.; Wintenberger, M.; Philippot, E. *J. Solid State Chem.* **1981**, *39*, 39.

(34) Zang, Y.; Dong, Y.; Que, L. Jr.; Kauffmann, K.; Munck, E. *J. Am. Chem. Soc.* **1995**, *117*, 1169.

(35) Fruchart, D.; Montmory, M. C.; Bertaut, E. F.; Bernier, J. C. *J. Phys.* **1980**, *41*, 141.

(36) Hoppe, R.; Brachtel, G.; Jansen, M. *Z. Anorg. Allg. Chem.* **1975**, *417*, 1; Greedan, J. E.; Raju, N. P.; Davidson, I. J. *J. Solid State Chem.* **1997**, *128*, 209.

(37) Goodson, P. A.; Oki, A. R.; Glerup, J.; Hodgson, D. J. *J. Am. Chem. Soc.* **1990**, *112*, 6248.

(38) McGrady, J. E.; Stranger, R. *J. Am. Chem. Soc.* **1997**, *119*, 8512.

are for M = Cr, Mn, and Fe. Redox chemistry prevents the formation for M = Ti and V while the M = Co material does not exist for $p_{O_2} \leq 1$ atm. Other trivalent ions, M = Y, In, and Sc, appear to be too large. The most remarkable feature of the structure are chains of edge-sharing MO_6 octahedra in which the two M−O−M bridging angles are highly asymmetric, differing by as much as 20° for M = Mn. In addition, the M−M distance is constant with M at 2.97 Å. This is attributed to the rigid nature of the BO_3 groups which bridge adjacent octahedra along the chains. As a result of these octahedral chains in the $PbMBO_4$ structure, one-dimensional magnetic behavior was anticipated and observed. For M = Cr and Fe, antiferromagnetic intrachain coupling was observed while, in the Mn phase, the intrachain coupling was ferromagnetic. Analysis of neutron diffraction data indicated that the interchain correlations were always ferromagnetic. Thus, $PbMnBO_4$ was shown to be an insulating ferromagnet, one of only a very small number of such materials. Values for the intrachain exchange coupling constants, J/k_B, were estimated from fits of the susceptibility data to standard models. These values were difficult to rationalize in comparison with the available, but limited, magnetostructural correlations and calculations. J/k_B was too small for both M = Cr and Fe and the ferromagnetic value for the Mn case is unexpected.

Acknowledgment. This work was supported by research grants from the Natural Sciences and Engineering Research Council of Canada to J.E.G. and J.B. H.P. also acknowledges the support from the Ontario government in the form of an Ontario Graduate Scholarship. The single-crystal X-ray data were collected by Dr. J. Britten in the Department of Chemistry at McMaster University. Hina Ghazi carried out some of the syntheses described and Dr. R. Hammond of the Neutron Program for Materials Research of the National Research Council of Canada assisted in the collection of the neutron diffraction data.

CM0217452